5 Understanding The Hubbard Model With Simple Calculations

Richard T. Scalettar
University of California Davis
Department of Physics and Astronomy, One Shields Ave., Davis, CA 95616

Contents

1 Introduction

The Hubbard Hamiltonian,

$$\hat{\mathcal{H}} = -t \sum_{\langle \mathbf{jl} \rangle \sigma} \left(\hat{c}^\dagger_{\mathbf{l}\sigma} \hat{c}_{\mathbf{j}\,\sigma} + \hat{c}^\dagger_{\mathbf{j}\,\sigma} \hat{c}_{\mathbf{l}\sigma} \right) + U \sum_{\mathbf{l}} (\hat{n}_{\mathbf{l}\uparrow} - \frac{1}{2})(\hat{n}_{\mathbf{l}\downarrow} - \frac{1}{2}) - \mu \sum_{\mathbf{l}} \hat{n}_{\mathbf{l}\sigma} \tag{1}$$

describes the 'hopping' of two species of fermions, spin $\sigma =\uparrow, \downarrow$, on neighboring sites $\langle \mathbf{jl} \rangle$ of a lattice, and interacting, when on the same site l, with an energy U. Here $\hat{n}_{\mathbf{l}\sigma\mathbf{e}} = \hat{c}^\dagger_{\mathbf{l}\sigma} \hat{c}_{\mathbf{l}\sigma}$ is the fermion number operator and μ is the chemical potential. I am going to assume familiarity with the basic properties of fermion creation and destruction operators $\hat{c}^\dagger_{\mathbf{l}\sigma}$ and $\hat{c}_{\mathbf{l}\sigma}$, including, for example, their anticommutation relations, $\left\{ \hat{c}^\dagger_{\mathbf{l}\sigma}, \hat{c}_{\mathbf{j}\sigma'} \right\} = \delta_{\mathbf{jl}} \delta_{\sigma\sigma'}$ and $\left\{ \hat{c}^\dagger_{\mathbf{l}\sigma}, \hat{c}^\dagger_{\mathbf{j}\sigma'} \right\} = 0$. We have written the interaction in 'particle-hole symmetric form'. This corresponds, up to an irrelevant constant term in the energy, to a a simple shift in the chemical potential μ from the alternate expression $U \sum_{\mathbf{l}} \hat{(} n_{\mathbf{l}\uparrow} \hat{n}_{\mathbf{l}\downarrow}$. We will see why this is more symmetric in Section 6, and the deep implications of such symmetries in Section 7.

A discussion of the Hubbard Hamiltonian is a truly immense undertaking. From a temporal point of view it encompasses a six decade history spanning the work of Hubbard, Anderson and Mott in the 1960's through a host of materials to which it has been applied: transition metal oxides, heavy fermions, cuprate superconductors, etc [1]. Indeed, in the last 15 years a major focus of the Atomic and Molecular (AMO) community has been on realizing and characterizing the Hubbard model in systems of ultracold atoms [2, 3]. Attempts to solve the Hubbard model computationally have driven a rich set of stories in inhomogeneous Hartree-Fock (magnetism and stripe formation) [4], Quantum Monte Carlo (QMC) [5] (including antiferromagnetic order, d-wave superconductivity, and the 'sign problem'), density matrix renormalization group (DMRG) methods (stripes and superconductivity) [6], and machine learning (ML) [7]. A recent review summarizes the breadth of these developments, applications and connections [8].

From a pedagogical point of view, then, the danger of a lecture (or even several lectures) on the Hubbard model is the temptation to focus on sophistacated techniques and applications. The audience can easily be left with a sense of the breadth and excitement of the field, but not with a concrete ability to '*do something*'.

The objectives of this lecture are to provide some specific calculations which shed light on the basic physics of the Hubbard model. We will begin with the non-interacting limit, i.e. obtaining the 'band structure' of the Hubbard model. We will emphasize that this already allows contact with some fascinating phenomena- localization by disorder, Fermi surface nesting and a divergence of the density of states linked to magnetism and superconductivity, and flat bands in which the electron energy is independent of momentum.

We will also describe two very interesting aspects of the non-interacting case. First, we will consider what happens when the motion of fermions to the left and to the right is unbalanced (the 'Hatano-Nelson' model). In this case the Hamiltonian is non-Hermitian (!!). Second, we

will relate a special choice of hoppings which can realize the surprising phenomenon of 'perfect quantum state transfer'.

After discussing the $U = 0$ limit, and these two interesting situations, we will examine the opposite limit when $t = 0$, or, more generally, the strong coupling case $U >> t$. This will give us insight into a fundamental feature of the Hubbard model, the 'Mott plateau', where the density gets frozen at half-filling for an extended range of chemical potential, a signature of an insulating phase arising from interactions.

The final objective is to describe the consequences of a set of canonical transformations which can be performed on the Hubbard model. We will see these allow us to discern surprising and not immediately intuitive physics in some parameter regimes from the more evident physics in others. Our first illustration will be on the by now well-known connections between magnetism in the repulsive Hubbard models and s-wave superconductivy and charge density wave formation in the attractive Hubbard model. We will then turn to a recent discovery of a transformation which leads to a rigorous demonstration of pair density wave formation, a phase of matter which has proven elusing to achieve both experimentally and theoretically.

2 A classical mechanics prelude

Let's begin with a familiar, but seemingly completely unrelated problem, which will prove to have close mathematical analogies with the non-interacting Hubbard model. Consider a one-dimensional array of N uniform masses m connected to their neighbors by uniform springs γ. Newton's equations of motion for this mass-spring system are,

$$m\frac{d^2x_l}{dt^2} = -\gamma\big(\, x_l - x_{l+1}\,\big) - \gamma\big(\, x_l - x_{l-1}\,\big)\,, \tag{2}$$

where $x_l(t)$ is the displacement from equilibrium of mass l at time t. We will not boldface the site indices when we are in one dimension. We solve this problem with the *ansatz* $x_l(t) = a_l\, e^{i\omega t}$ which reduces the N coupled differential equations to N coupled algebraic equations for the amplitudes a_l. After cancelling the common factor of $a_0\, e^{i\omega t}$ from all the terms, we find

$$m\,\omega^2\, a_l = \gamma\big(\, a_l - a_{l+1}\,\big) + \gamma\big(\, a_l - a_{l-1}\,\big)\,. \tag{3}$$

These equations are solved by introducing normal mode coordinates labeled by k,

$$a_l = e^{-ikl}a_0, \tag{4}$$

yielding the normal mode frequencies,

$$\omega^2(k) = 2\gamma\big(1 - \cos(k)\big)\,. \tag{5}$$

Here we have now used notation emphasizing the frequency depends on the 'momentum' k. (We will come back shortly to why calling k the momentum makes sense.)

Eq. 5 is an embarassment of riches. From a collection of N linear equations (Eqs. 3) we have an *infinite* set of solutions labeled by the continuous parameter k. Something is wrong, and it's because we did not treat the boundary conditions carefully. Equations 3 are only true for the masses which have both left and right neighbors, $l = 2, 3, \cdots N$-1. The two masses at the end have only a single neighbor if we adopt 'open boundary conditions' (obc). Here instead we use 'periodic boundary conditions' (pbc), and link oscillator $l = 1$ to oscillator $l = N$ with an extra spring of potential energy $\frac{1}{2}\gamma(x_1 - x_N)^2$. Then Eqs. 3 apply to *all* x_l, but only if we demand that $x_0 \equiv x_N$ and $x_1 \equiv x_{N+1}$.

This solves our problem of too many solutions, since it quantizes the previously unrestricted allowed values of momentum by requiring $e^{ikN} = 1$ or, in other words, $k \in \frac{2\pi}{N}\{1, 2, \cdots, N\}$. Because cosine is periodic, it is equivalent to set $k = \frac{2\pi}{N}\{-\frac{N}{2} + 1, -\frac{N}{2} + 2 \cdots \frac{N}{2}\}$. which has the advantage of making k symmetric about $k = 0$.

It is useful to consider two special cases. When $k = 0$, all masses have identical displacements $a_l = a_0$. The entire chain is shifted rigidly and $\omega(k) = 0$. This is an example of a zero frequency 'Goldstone mode' associated with the translational invariance of our mass-spring system. Because only inter-mass springs are present, there is no potential tying any mass to a particular location in space. As a consequence the energy is invariant under a simultaneous translation of all the masses. Put another way, the choice of origin is irrelevant, the equations are unchanged by a constant shift of all the coordinates, $x_l \to x_l + c$. On the other hand, when $k = \pi$ the masses alternate $a_l = a_0\, e^{i\pi l} = a_0(-1)^l$. This results in the largest normal mode frequency (energy), $\omega^2 = \frac{4k}{m}$. There is an interesting analogy with quantum mechanics here. If you sketch a_l versus l for this highest energy mode, you see there is a node between every mass. a_l wiggles as fast as possible. Similarly, in quantum mechanics we know that wiggly wave functions are associated with *high* kinetic energy.

One can also solve the obc case. The 'dispersion relation' giving the functional form for $\omega(k)$ is unchanged, but the N allowed momenta are shifted slightly to $k \in \frac{2\pi}{N+1}\{0, 1, 2, \cdots N\text{-}1\}$. The pbc case is a bit more simple, so we use it here. Besides simplicity, it is also the case that properties measured in finite length N chains with pbc are closer to the thermodynamic limit $N = \infty$ than obc. Specifically, finite size corrections often go as $\frac{1}{N^2}$ with pbc and $\frac{1}{N}$ with obc.

A closing observation is that this solution of coupled oscillators all goes horribly wrong in the presence of anharmonicity. Indeed, even a single anharmonic oscillator, the solution of $F = ma$ with $V(x) = \frac{1}{2}kx^2 + \frac{1}{4}ux^4$ is intractable. As we shall see below, the presence of interactions, quartic terms in the fermion creation and destruction operators, $U\hat{n}^\dagger_{l\uparrow}\hat{n}_{l\downarrow} = U\hat{c}^\dagger_{l\uparrow}\hat{c}_{l\uparrow}\hat{c}^\dagger_{l\downarrow}\hat{c}_{l\downarrow}$, analogous to the fourth power ux^4, is precisely what makes the Hubbard model impossible to solve for U non-zero.

That's a long time spent on classical mechanics! But we will see now that the exact same mathematics underlies the solution of the non-interacting Hubbard model.

3 The Hubbard Model at $U = 0$

3.1 The 1D Case (linear chain)

Let's write down the non-interacting ($U = 0$) Hubbard model for a 1D chain.

$$\hat{\mathcal{H}} = -t \sum_l \left(\hat{c}_l^\dagger \hat{c}_{l+1} + \hat{c}_{l+1}^\dagger \hat{c}_l \right) - \mu \sum_l \hat{c}_l^\dagger \hat{c}_l \tag{6}$$

Because we will not have any interactions for this Section, we have suppressed the spin index σ on the fermionic operators. That is, since U is the only thing that connects fermions with $\sigma =\uparrow$ to fermions with $\sigma =\downarrow$, when $U = 0$ we can just solve each spin sector independently.

Now just as we defined normal mode coordinates for the positions of our masses we can also here define linear combinations of

$$\hat{c}_k^\dagger \equiv \frac{1}{\sqrt{N}} \sum_l e^{ikl}\, \hat{c}_l^\dagger \tag{7}$$

and its inverse,

$$\hat{c}_l^\dagger \equiv \frac{1}{\sqrt{N}} \sum_l e^{-ikl}\, \hat{c}_k^\dagger. \tag{8}$$

Note the reemblance between Eqs. 7 and 4. The fermion creation operator transformation is, however, a little more subtle than the classical mechanics case, because we must be sure that our new operators $\hat{c}_k$ obey the same fermionic anti-commutation relations as the originals. It is easy to prove this from the identities

$$\frac{1}{N} \sum_l e^{i(k-k')l} = \delta_{kk'} \tag{9}$$

and

$$\frac{1}{N} \sum_k e^{i(l-l')k} = \delta_{ll'} \tag{10}$$

which hold for the discrete allowed momenta $k, k' \in \frac{2\pi}{N}\{-\frac{N}{2}+1, -\frac{N}{2}+2 \cdots \frac{N}{2}\}$. Equations 9 and 10 are the discrete analogs of the familiar orthogonality relations used in Fourier transforms.

We refer to a change of operators which preserves the commutation relations, such as Eq. 7, as a canonical transformation. This too is analogous language to classical mechanics, where a canonical transformation preserves the Poisson brackets. The last section of this Chapter will focus on this topic.

Plugging the transformation Eq. 8 into the Hamiltonian, Eq. 6, and making use of Eqs. 9 and 10 yields

$$\hat{\mathcal{H}} = \sum_k \left(E(k) - \mu \right) \hat{c}_k^\dagger \hat{c}_k \tag{11}$$

where

$$E(k) = -2t\cos(k) \tag{12}$$

The similarity between the right-hand sides of Eqs. 5 and 12 should be evident, from the appearance of $\cos(k)$ and the identification $2\gamma \leftrightarrow -\mu$. The energy levels of the 1D Hubbard chain range from $-2t \leq E(k) \leq +2t$. One refers to this range as the (1D chain) 'bandwidth' $W = 4t$.

It is interesting to think about the physics of the structure on Eq. 11. The Hamiltonian does not 'mix' different values of momentum k. When an electron of momentum k is destroyed, all that can happen is that an electron with the *same* momentum be created. This is the analog of the classical mechanical principal that normal modes do not mix: A system set into oscillation in a particular normal mode remains in that mode forever, and none of the others ever get excited.

Concerning the left-hand sides, one can wonder why the frequency/energy appears linearly in Eq. 12 in the quantum problem, whereas it was quadratic in the coupled oscillator calculation Eq. 5. The answer, of course, lies in the fact that Newton's equations involve $\frac{d^2}{dt^2}$, whereas the Schroedinger equation involves only $\frac{\partial}{\partial t}$.

We have exploited the translation invariance of the oscillator system and the Hubbard Hamiltonian to guess (make an *ansatz*) to extract the normal modes/band structure. In the absence of such symmetries the problem becomes one of diagonalizing a matrix.

Put another way, we can write the Hubbard Hamiltonian as

$$\hat{\mathcal{H}} = \begin{pmatrix} \hat{c}_1^\dagger & \hat{c}_2^\dagger & \hat{c}_3^\dagger & \hat{c}_4^\dagger & \hat{c}_5^\dagger & \cdots \end{pmatrix} \begin{pmatrix} -\mu & -t & 0 & 0 & 0 & \cdots \\ -t & -\mu & -t & 0 & 0 & \cdots \\ 0 & -t & -\mu & -t & 0 & \cdots \\ 0 & 0 & -t & -\mu & -t & \cdots \\ 0 & 0 & 0 & -t & -\mu & \cdots \\ \vdots & \vdots & \vdots & \vdots & \vdots & \ddots \end{pmatrix} \begin{pmatrix} \hat{c}_1 \\ \hat{c}_2 \\ \hat{c}_3 \\ \hat{c}_4 \\ \hat{c}_5 \\ \vdots \end{pmatrix} \tag{13}$$

We happen to know (if we have some experience with tri-diagonal matrices) the eigenvalues and eigenvectors of the matrix in Eq. 13. The eigenvalues are just the $E(k)$ in Eq. 12, and the matrix of eigenvectors has entries $\Psi_{kl} = e^{ikl}$. I have used the notation Ψ deliberately, because these eigenvectors are quite literally the familiar plane-wave solutions of the free particle Schroedinger equation (on a discrete lattice). This justifies our referring to k as the momentum.

If we had not known this similarity transformation, we would have proceeded by diagonalizing the matrix by calling an appropriate BLAS/LAPACK routine. While we should avoid solving the eigenproblem numerically if an analytic solution is available, it is worth emphasizing it is not at all a big deal. We shall see the utility of this way of thinking in terms of matrix diagonalization when we discuss localized modes in the non-interacting Hubbard model.

Equation 12 gives the energy of a single electron, that is the energy of the state $|k\rangle = c_k^\dagger|\text{vac}\rangle$. It remains to discuss the computation of the energy with M electrons. The prescription is sim-

ple: if several electrons are present, the state $|\, k_1\, k_2\, \cdots k_M\, \rangle = c^\dagger_{k_1} c^\dagger_{k_2} \cdots c^\dagger_{k_M} |\mathrm{vac}\rangle$ has energy $E(k_1) + E(k_2) + \cdots E(k_M)$. Of course the Pauli principle forbids any of the k_i from being the same for a given spin species.

If we are interested in the ground state of M electrons, we fill up (occupy) the states of lowest energy. The 'Fermi Energy' is the highest energy that is occupied for M particles. The seemingly mysterious choice of the minus sign in front of the hopping parameter t makes momentum $k = 0$ have the lowest energy, with a Fermi surface enclosing it.

Once we have the dispersion relation in hand, a very important quantity is the density of states $N(\omega)$. In words, $N(\omega)d\omega$ gives the number of $E(k)$ values which lie between ω and $\omega + d\omega$. Formally,

$$N(\omega) \equiv \frac{1}{N} \sum_k \delta\big(\, \omega - E(k) \,\big) \tag{14}$$

We can easily get $N(\omega)$ in the limit $N \to \infty$ where the k values become continuous

$$N(\omega) = \frac{1}{2\pi} \int_{-\pi}^{+\pi} dk\, \delta\big(\, \omega + 2t\cos(k) \,\big) = \frac{1}{\sqrt{4t^2 - \omega^2}} \tag{15}$$

We have used the presciption $\frac{1}{N}\sum_k \to \frac{1}{2\pi}\int dk$ in going from a sum over discrete values separated by $\frac{2\pi}{N}$, to an integral. $N(\omega)$ diverges at $\omega = \pm 2t$ where the dispersion relation $E(k) = -2t\cos(k)$ is flat, an observation familiar from textbook discussions of band theory.

3.2 The 2D Square Lattice

On a 2D square lattice, the noninteracting Hubbard Hamiltonian is

$$\hat{\mathcal{H}} = -t \sum_{l_x, l_y} \big(\, \hat{c}^\dagger_{l_x, l_y} \hat{c}_{l_x+1, l_y} + \hat{c}^\dagger_{l_x+1, l_y} \hat{c}_{l_x, l_y} + \hat{c}^\dagger_{l_x, l_y} \hat{c}_{l_x, l_y+1} + \hat{c}^\dagger_{l_x, l_y+1} \hat{c}_{l x, l_y} \,\big) - \mu \sum_{l_x l_y} \hat{c}^\dagger_{l_x, l_y} \hat{c}_{l_x, l_y} \tag{16}$$

Although it is useful to work through the algebra for practice, the result is pretty reasonable, and we will just quote it. The process is just to redo the steps of Sec. 2.1 with $l \to l_x, l_y$. The result is

$$\hat{\mathcal{H}} = \sum_{k_x, k_y} \big(\, E(k_x, k_y) - \mu \,\big) \hat{c}^\dagger_{k_x, k_y} \hat{c}_{k_x, k_y} \tag{17}$$

where

$$E(k_x, k_y) = -2t\cos(k_x) - 2t\cos(k_y) \tag{18}$$

gives the energy of an electron of momentum k_x, k_y. The energy levels of the Hubbard model on a square lattice range from $-4\,t \le E(k_x, k_y) \le +4\,t$. The bandwidth $W = 8\,t$.

For many fermions, we again get the energy by just summing up the single particle levels out to a maximum Fermi Energy. However, in $d > 1$ one can ask for the shape of the contour of

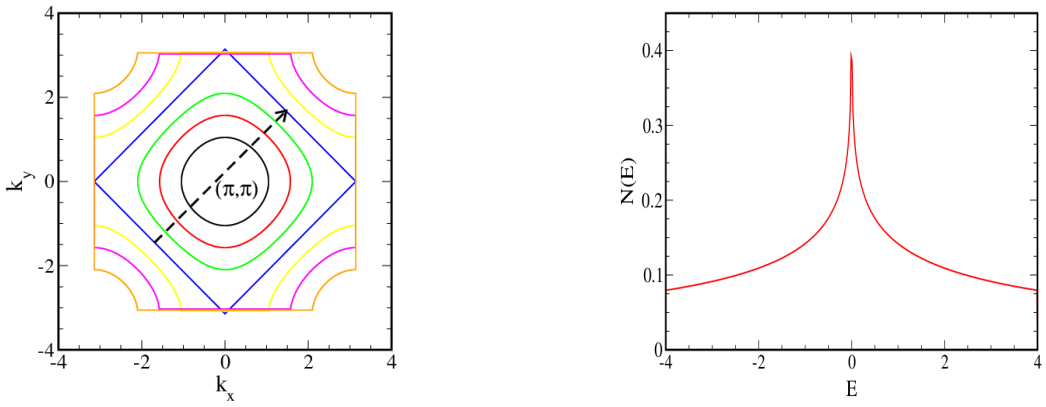

Fig. 1: *Left: The Fermi surfaces of the Hubbard model an a square lattice with nearest neighbor hopping for different numbers of particles (filling). They begin as circles at low density but evolve into a rotated square at half-filling. Right: The density of states $N(\omega)$ of the Hubbard model an a square lattice with nearest neighbor hopping. There is a divergence ('van Hove singularity') of $N(\omega)$ at $\omega = 0$ (half filling).*

the boundary between the occupied and unoccupied k_x, k_y. This is referred to as the 'Fermi surface' (FS). For small k_x, k_y we can expand the cosines in Eq. 18 and

$$E(k_x, k_y) \sim -4t + t\,(\,k_x^2 + k_y^2\,) \tag{19}$$

and the FS is a circle about $(k_x, k_y) = (0, 0)$. Thinking in analogy with $E(k) = \hbar^2(k_x^2+k_y^2)/2m$ we see that the effective mass of the fermions $m = 1/(2t)$ (setting $\hbar = 1$).

In general $E(k)$ is not quadratic and the FS does not have a circular topology (sphere in three dimensions). Indeed, the FS's for different fillings (number of fermions) are shown in the left panel of Fig. 1. An interesting feature of the dispersion relation of Eq. 18 is 'perfect nesting'. As seen in the left panel of Fig. 1, when the interior of the FS encompasses half of the allowed momenta (and hence the lattice is half-filled), the FS is a 'rotated square' and has the feature that a single wave-vector $(k_x, k_y) = (\pi, \pi)$ connects many points on the FS. The second is a 'van Hove singularity' in the density of states. At half-filling, $N(\omega = 0)$ diverges. See the right panel of Fig. 1.

It turns out that both of these properties make the square lattice Hubbard model particularly prone to assuming ordered phases when the interaction U is turned on. The rough reason appeals to your knowledge of second order perturbation theory, where you know the effect of a perturbation $\hat{V}$ is to shift the energy E_n of eigenstate $|n\rangle$ by $E_n^{(2)} = \sum_{m\neq n} \frac{|\langle n|\hat{V}|m\rangle|^2}{E_n - E_m}$. If there are many states with $E_m = E_n$ the effect of $\hat{V}$ will be very large. This is precisely what happens with perfect nesting. The van-Hove singularity in $N(\omega)$ has been suggested to be implicated in high superconducting transition temperatures. That is, thinking of the BCS formula for the critical temperature in terms of the coupling constant λ and the density of states, $T_c \sim e^{-1/\lambda N(\omega)}$, we see that a large $N(\omega)$ suggests a large T_c.

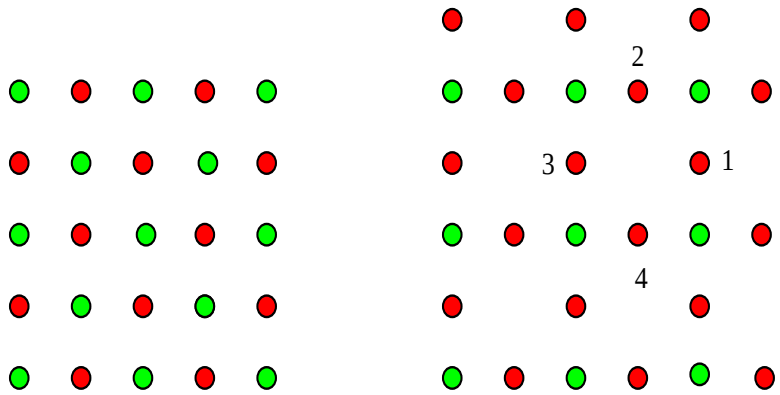

Fig. 2: *Left: The square lattice can be decomposed into two groups $\mathcal{A}$ and $\mathcal{B}$ of sites, colored as red and green, such that the neighbors of a red site are only green and vice-versa. The geometry is said to be 'bipartite'. Right: The Lieb lattice is also bipartite, but note there are twice as many red sites as green sites.*

We conclude by noting that there are materials, like the cuprate superconductors, for which the square lattice is considered appropriate: the copper atoms in the CuO_2 planes reside on a square lattice.

3.3 The Lieb Lattice and "Flat Bands"

An interesting feature of the square lattice is that its sites can be divided into two sublattices (red and green in the left panel of Fig. 2) such the near neighbors of red sites are always green and the near neighbors of green sites are always red. Such a geometry is said to be 'bipartite'. This property has deep implications for the physics, most fundamentally its consistency with antiferromagnetic order. In a model where the energy is minimized by neighboring spins pointing in opposite directions, one can place the electrons so that those with up spins occupy one sublattice and those with down spins reside on the other sublattice with no frustration (neighboring sites with high energy because their spins are in the same direction).

The honeycomb lattice describing the positions of the carbon atoms in a sheet of graphene is also bipartite. In both the square and honeycomb cases, the numbers of red and green sites are identical. We will next consider the Hubbard model on a Lieb lattice, shown in the right panel of Fig. 2. Although we blitzed through going from a 1D chain to a 2D square lattice, it is worth being a bit more careful with this one, because going to momentum space does not quite complete the process of diagonalization.

Aside: The serious student of the Hubbard model would do well to compute $E(k_x, k_y)$ for a honeycomb geometry. This is useful 'technical' practice, as dealing with axes which are not parallel to $\hat{x}$ and $\hat{y}$ requires some care. It is also of course important physically towards the understanding of graphene. Just as the dispersion relation of the square lattice has interesting properties like Fermi nesting, the honeycomb lattice hosts Dirac fermions, electrons whose kinetic energy is linear in their momenta.

For the Lieb lattice, the repeating structure contains a three atom basis. In transforming to momentum space we must include a 'band' index for the basis, in addition to momentum. The resulting Hamiltonian is diagonal in (k_x, k_y) but the three basis states of given (k_x, k_y) mix with the 3x3 matrix.

$$\begin{pmatrix} 0 & -t\left(1+e^{ik_x}\right) & -t\left(1+e^{ik_y}\right) \\ -t\left(1+e^{-ik_x}\right) & 0 & 0 \\ -t\left(1+e^{-ik_y}\right) & 0 & 0 \end{pmatrix} \tag{20}$$

Diagonalizing this matrix completes the process of identifying the single particle states. The crucial and surprising feature is that one of the energy bands has $E(k_x, k_y) = 0$. The (kinetic) energy is independent of momentum. A plot of energy versus momentum yields a horizontal line, i.e. a 'flat band'.

One can actually understand the origin of the zero energy states in real space. Consider the four sites enumerated as $1, 2, 3, 4$ in Fig. 2((right). Imagine a wavefunction with nonzero components only on these four sites, and make those components all of equal magnitude, but alternating in sign so that the entries for sites $1, 3$ are positive and those for $2, 4$ are negative. It is fairly easy to see that if you apply the real space Hamiltonian matrix of Eq. 13, but generalized to hopping on the Lieb lattice, the result is the zero vector: Because only sites $1, 2, 3, 4$ have nonzero components. hopping is possible only to the four green sites which adjoin them. However, because of the sign alternation of the components in the original vector, there is a perfect cancellation of the hopping. It is clear that this numbering $1, 2, 3, 4$ can be performed around *any* of the 'holes' in the Lieb geometry. There is an eigenvector of zero eigenvalue for each unit cell.

The Lieb lattice is also often considered as a more refined picture of the cuprates, because the oxygen atoms of a CuO_2 sheet lie on the midpoints of the bonds of the square array of copper atoms, just as the red circles in Fig. 2. The flat band is entirely of 'oxygen' origin, as the construction above demonstrates.

3.4 Localization by Disorder

Examining Eqs. 6 and 13, it is clear that disorder in the chemical potentials (making the energy for a fermion to occupy a particular location site-dependent) can be simply incorporated by changing the matrix elements $\mu \rightarrow \mu_l$. The transformation Eq. 7 no longer diagonalizes the Hamiltonian, as translation invariance is broken. However the diagonalization can still be accomplished numerically.

A very interesting phenomenon occurs. While the plane wave eigenstates in the absence of randomness extend throughout the lattice, the eigenstates in the presence of disorder can be 'localized', meaning that the components of the eigenstate are significant only on a fraction of the sites and exponentially small elsewhere.

Figure 3 shows the square of the ground state wavefunction for a 1D chain of $N = 1024$ sites for different ranges Δ of the random chemical potential (site energy) $-\Delta/2 < \mu_l < +\Delta/2$ and no interactions ($U = 0$). Wave functions have been shifted so that their maximum amplitude

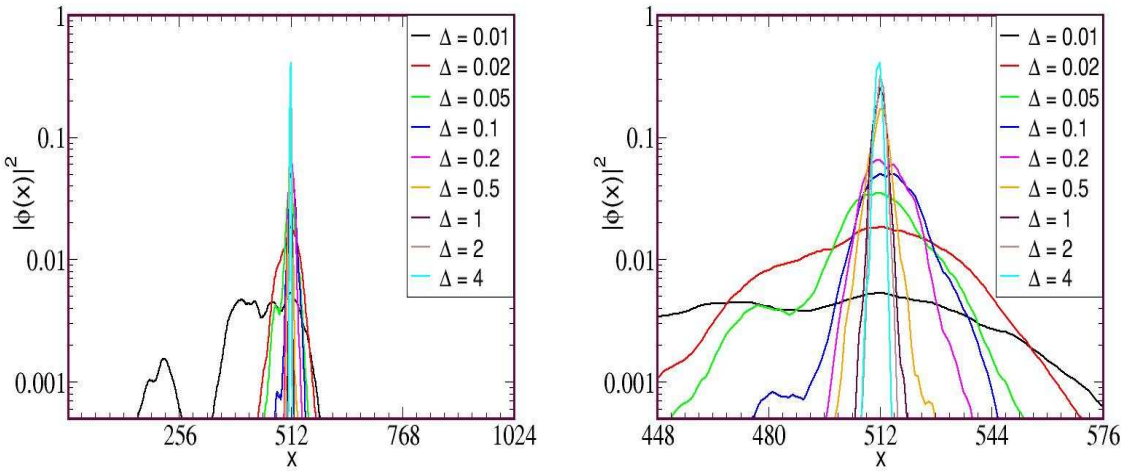

Fig. 3: *Left: Square of amplitude of the ground state wavefunction for a disordered 1D chain. As the disorder amplitude Δ decreases, the wavefunction is increasingly spread out, but it remains localized for any nonzero Δ. Right: Same data put blown up near the lattice center. Note the logarithmic scale on the vertical axes.*

is at the lattice center $x = N/2 = 512$. In 1D all wavefunctions fall off exponentially for an arbitrarily small Δ. The same is true in 2D, though it was a very challenging assertion to prove [9]. In 3D, the eigenstates near the center of the DOS are delocalized, and those at the edges (high and low energies) are localized. The energy separating these cases is referred to as the 'mobility edge.' Detailed numerical work is reviewed in [10].

Here one can continue the analogy with classical systems. A beautiful discussion of Maradudin describes localization about a single defect mass in a 1D mass-spring chain [12].

There is a lot to unpack in the comments above, and indeed there was a long effort to understand the nature of localization in two dimensions. Indeed, a major theme of condensed matter physics for nearly three decades concerned whether non-zero U could result in delocalization in 2D [11]. But the main message for us here is that many aspects of this deep and beautiful chapter of condensed matter physics conform to the title of this chapter: From a computational perspective they boil down to the very familiar and simple question of diagonalizing a matrix!

4 The Hatano-Nelson model

A recently emerging area of interest concerns non-Hermitian Hamiltonians [13–15]. The simple methods we have introduced give us a foothold into this field as well. For concreteness, let's consider the 'Hatano-Nelson Hamiltonian' in one dimension:

$$\hat{\mathcal{H}} = -t \sum_{l=1}^{L} (e^{h}\, \hat{c}_{l+1}^{\dagger} \hat{c}_l + e^{-h}\, \hat{c}_l^{\dagger} \hat{c}_{l+1}) + \sum_l \mu_l\, \hat{c}_l^{\dagger} \hat{c}_l \quad . \tag{21}$$

which is obtained from the Hubbard model of Eq. 6 by introducing a hopping which is different for fermions moving to the left and to the right. The parameter h controls the degree of anisotropy in the hopping, and μ_l are random site energies. Periodic boundary conditions connect sites 1 and L.

In the case where there is no disorder, $\mu_l = 0$, we can try the same canonical transformation as Eq. 7, which leads to eigenvalues then have the form,

$$E(k) = -t\,(e^{-h-ik} + e^{h+ik}) = -2t\cosh(h)\cos(k) - 2t\sinh(h)\sin(k)\ . \tag{22}$$

As k varies from 0 to 2π (in steps of $\frac{1}{L}$) this describes an ellipse centered at the origin of the complex plane. The length of the ellipse along the real axis is $4t\cosh(h)$ and along the imaginary axis, $4t\sinh(h)$. The periodic boundary conditions are crucial. Without them one can do a 'gauge transformation', or in more elementary language a redefinition of the eigenvectors, which makes h disappear from the problem: $\tilde{v}_l = e^{-hl}v_l$. Then the matrix is Hermitian, with all real eigenvalues.

As remarked earlier, in the presence of disorder the transformation of Eq. 7 no longer works. Instead one simply diagonalizes the matrix,

$$H = \begin{pmatrix} \mu_1 & -t\,e^{h} & 0 & 0 & 0 & \cdots & -t\,e^{-h} \\ -t\,e^{-h} & \mu_2 & -t\,e^{h} & 0 & 0 & \cdots & 0 \\ 0 & -t\,e^{-h} & \mu_3 & -t\,e^{h} & 0 & \cdots & 0 \\ \vdots & \vdots & \vdots & & & \vdots & \ddots \\ -t\,e^{h} & 0 & 0 & 0 & 0 & -t\,e^{-h} & \mu_L \end{pmatrix}\ . \tag{23}$$

When disorder is present, the original elliptical distribution in the complex plane develops 'wings' extending out along the real axis. See Fig. 4. The eigenvectors associated with the real eigenvalues on the wings are localized, and those on the wings are real. The plausibility argument for this assertion is that one can accumulate the h factors on any desired link (or set of links) through the gauge transformation noted above. For a localized eigenvector one can move all the h factors to a lattice location where the wave function is arbitrarily (exponentially) small. So those eigenvectors are governed by a piece of H which can be made Hermitian in the only part of the lattice that matters to them. Thus, they will have real eigenvalues. This doesn't work for extended eigenvectors, so they have complex eigenvalues.

The numerical results of Fig. 4 reveal some interesting general features of computational work on Hubbard models (and even more generally). Except for $h = 0.3, \Delta = 4.0$, $N = 1024$ is large enough that the results are 'self-averaging': The eigenspectra for different disorder realizations largely coincide. However, when h is small and the disorder is large enough, one begins to see significant variation from realization to realization (lower left panel of Fig. 4. The $N = 1024$ dimensional matrices can be diagonalized in about one half of a minute using the LAPACK routine *dgeevx*. Diagonalization scales as N^3 so $N = 4096$ would only take about a half-hour.

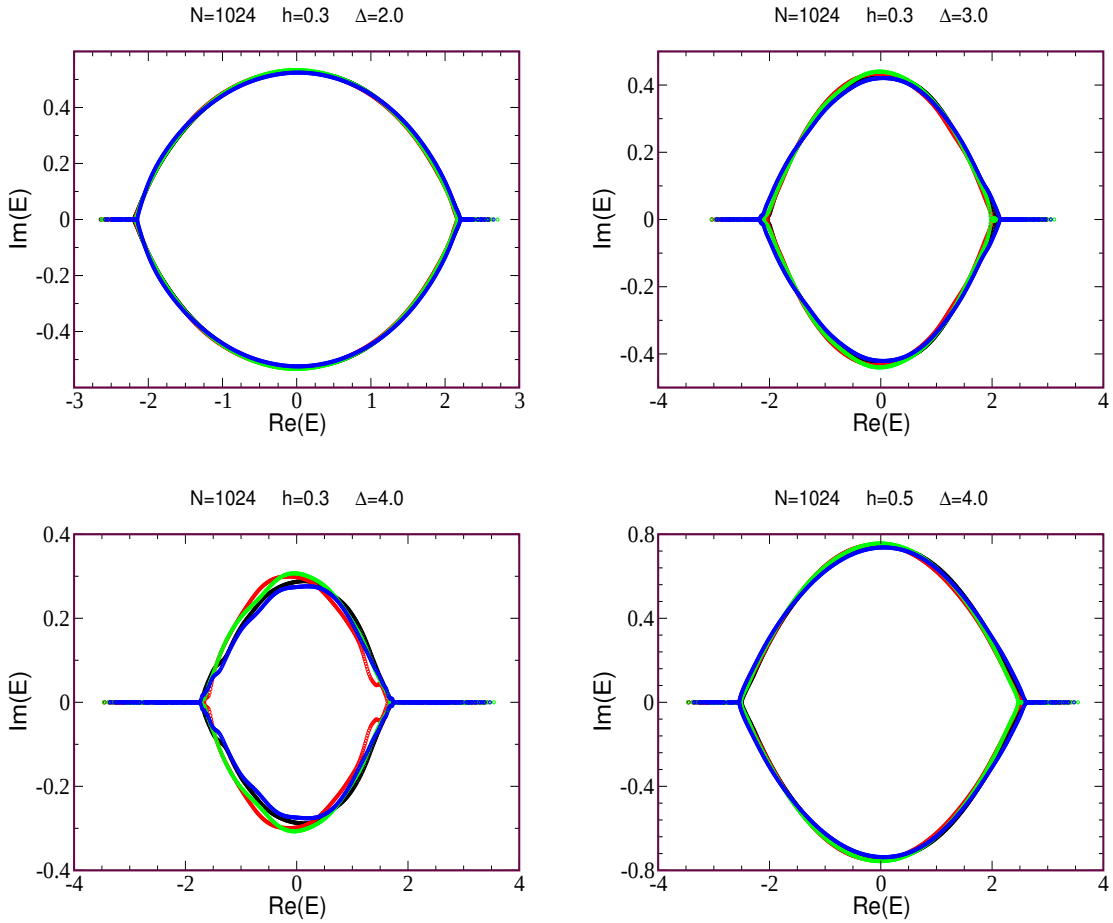

Fig. 4: *Eigenvalues of the Hatano-Nelson Hamiltonian for an $N = 1024$ site chain. The random chemical potentials are chosen from a box distribution $-\Delta < \mu_l < +\Delta$. Four disorder realizations are shown in each figure. As the disorder Δ increases at fixed h, the real 'wings' become longer. As h increases at fixed Δ, the imaginary part of the eigenvalues grows.*

5 Perfect Quantum state transfer

One of the most familiar and prominent aspects of quantum mechanics is the uncertainty principle. Our knowledge of the position and momentum of a quantum mechanical particle must obey $\Delta x \Delta p \geq \hbar/2$. Moreover, we expect uncertainties in position to grow in time ('spreading of the wave packet'). Consider a particle moving in $d = 1$ with no potential $V(x) = 0$. Contrast the motion of the 'slowest' part of the wave-packet at $x - \Delta x$ moving with momentum $p - \Delta p$, and the 'fastest' part of the wave-packet at $x + \Delta x$ moving with momentum $p + \Delta p$. The separation of the extremes grows as $2(\Delta x + t\, \Delta p)$. This provides a very crude picture for spreading, but this linear growth of uncertainty with time is not correct. Instead, $\Delta x \sim \sqrt{t}$ as can be seen by explicitly solving the free particle Schroedinger equation, or else simply by noting its similarity to the classical diffusion equation.

It is therefore remarkable that we can construct Hubbard models which exhibit 'perfect quantum

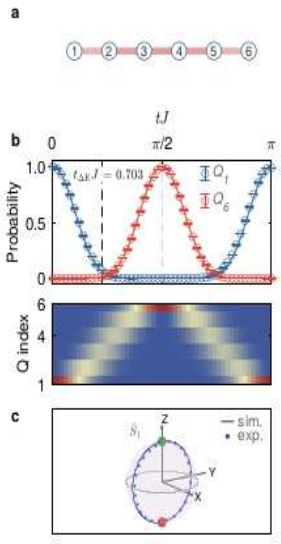

Fig. 5: (a,b): *Perfect quantum state transfer has been achieved experimentally in a collection of superconducting qubits with tunable couplings adjusted according to the prescription described in the text for a $N = 6$ site chain. The system starts with qubit $Q = 1$ excited, and the excitation is transferred to the other end of the chain $Q = 6$ at a time $t = \pi/(2J)$ later.* **(c):** *A picture of the time evolution from the angular momentum perspective. Image taken from [20].*

state transfer' (QST). That is, a wavefunction perfectly localized at one end of a $d = 1$ chain will, at later times, be perfectly localized at the opposite end! Although spreading does occur at intermediate times, the wave function somehow re-coalesces to have zero position uncertainty.

How is this (quantum mechanically) counter-intuitive result realized? We know that each eigenstate $|\phi_n\rangle$ of a quantum mechanical system evolves with a frequency $\omega_n = E_n/\hbar$, where E_n is its energy. A generic (localized) wave function will be a linear combination of the $|\phi_n\rangle$ and it seems plausible that to get a different localized wavefunction at later time, the frequencies ω_n must somehow be such that the maxima of the different waves can come into alignment. An obvious way that could happen is if the ω_n were equally spaced. We are thus led to think about whether we can find a tridiagonal matrix which has the property that the eigenvalues have constant separation. Uniform hoppings $t_{l,l+1} = t$ will not work, since, as we have seen, the resulting eigenvalues are $E(k) = -2t\cos(k)$.

A clever thought is this: The components of angular momentum operators have equally spaced levels. Consider $2\,\hat{S}_x = \hat{S}_+ + \hat{S}_-$ whose action on an eigenstate $|jm\rangle$ of $\hat{S}^2$ and $\hat{S}_z$ is $2\,\hat{S}_x|j,m\rangle = \sqrt{j(j+1)-m(m+1)}|j,m+1\rangle + \sqrt{j(j+1)-m(m-1)}|j,m-1\rangle$. Taking $j = 5/2$, there are six states with eigenvalues $2m\hbar = \{-5,-3,-1,+1,+3,+5\}\,\hbar$. Using the expression above, the state $|j,m\rangle$ is connected to its neighbors $|j,m+1\rangle$ and $|j,m-1\rangle$ with coefficients $\sqrt{5},\sqrt{8},\sqrt{9},\sqrt{8},\sqrt{5}$. (We have now set $\hbar = 1$.)

We also know the time evolution. A spin starting with z component of angular momentum $m = +5/2$, under the influence of $\hat{\mathcal{H}} = 2J\,\hat{S}_x$ will rotate to $m = -5/2$ in a time $t = \pi/(2J)$. A picture of this is provided in panel (c) of Fig. 5.

We now note that this mathematical structure of an operator connecting adjacent states (a tridiagonal matrix) is precisely that of the near-neighbor Hubbard kinetic energy operator in 1D. Translating the angular momentum formalism to this language, we see that if we had a six site chain with $\hat{\mathcal{H}} = -\sum_l t_{l,l+1}\left(\hat{c}^\dagger_{l+1}\hat{c}_l + \hat{c}^\dagger_l\hat{c}_{l+1}\right)$ and $t_{1,2} = \sqrt{5}J,\ t_{2,3} = \sqrt{8}J,\ t_{3,4} = \sqrt{9}J,\ t_{4,5} =$

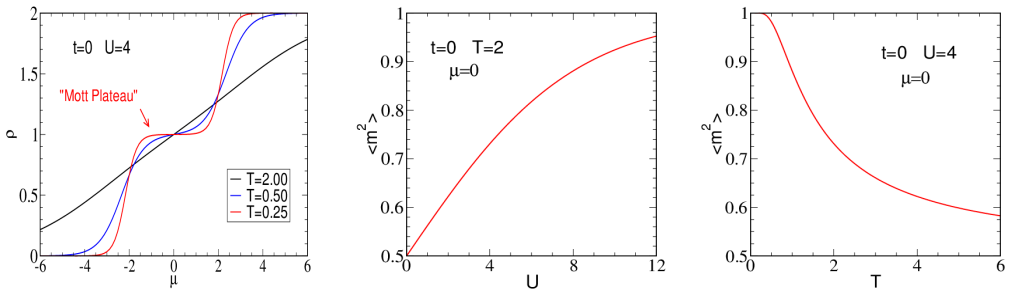

Fig. 6: *Left: The density ρ as a function of chemical potential for a single site with $U = 4$. As the temperature T is lowered, a Mott plateau develops. Center: The local moment $\langle \hat{m}^2 \rangle$ as a function of U at fixed temperature $T = 2$. Right: The local moment $\langle \hat{m}^2 \rangle$ as a function of T at fixed temperature $U = 4$. Local moments develop as either T is reduced or U is increased. Chemical potential $\mu = 0$ in the middle and right panels, so the site is half-filled.*

$\sqrt{8}J$, and $t_{5,6} = \sqrt{5}J$, the eigenenergies would be $\{-5, -3, -1, +1, +3, +5\}\, J$. The time evolution would be such that an electron beginning with $|\psi(t=0)\rangle = \hat{c}_1^\dagger |\text{vac}\rangle$ will evolve *perfectly* into $|\psi(t = \pi/(2J))\rangle = \hat{c}_6^\dagger |\text{vac}\rangle$.

We have thus constructed a hopping Hamiltonian which exhibits perfect Quantum State Transfer. The general rule for a chain of arbitrary length N is $t_{l,l+1} = \sqrt{l(N-l)}$ [16]. This prescription was first noted by Christandl [17] and later generalized by Kay [18].

6 The Strong Coupling Limit

We invested a lot of time on the non-interacting Hubbard model. It was time well-spent, since we saw there is a lot of very interesting physics, from nesting, to localization, to perfect Quantum State Transfer. But, of course we should not be satisfied with this $U = 0$ limit. In this section, we will consider the opposite extreme of strong coupling, $t = 0$, for which the Hubbard model becomes a collection of single sites

$$\hat{\mathcal{H}} = U \sum_{\mathbf{j}} (\hat{n}_{\mathbf{j}\uparrow} - \frac{1}{2})(\hat{n}_{\mathbf{j}\downarrow} - \frac{1}{2}) - \mu \sum_{\mathbf{j}} (\hat{n}_{\mathbf{j}\uparrow} + \hat{n}_{\mathbf{j}\downarrow}) \tag{24}$$

which can be considered independently.

Each site has four possible configurations: empty, having a single electron (either spin up or spin down) or doubly occupied. The states $|0\rangle, |\uparrow\rangle, |\downarrow\rangle, |\uparrow\downarrow\rangle$ are eigenstates of $\hat{\mathcal{H}}$ with eigenvalues $+U/4,\ -\mu - U/4,\ -\mu - U/4,\ +U/4 - 2\mu$ respectively. At this point we can see the meaning of the interaction term being 'particle-hole symmetric': the contribution of the interaction term in Eq. 24 to the state $|0\rangle$ with two *holes* is identical to that of the state with two *particles* $|\uparrow\downarrow\rangle$. An important consequence of this convention is that half-filling conveniently occurs always at

$\mu = 0$ for any value of temperature T and interaction strength U. Indeed, if we are on a bipartite lattice, this is true even if the hopping t is non-zero, as we shall see in the subsequent section.

The $t = 0$ partition function then consists of a term

$$Z = \sum_{\alpha} \langle \alpha | e^{-\beta \hat{\mathcal{H}}} | \alpha \rangle = e^{-\beta U/4} + 2e^{\beta\mu + \beta U/4} + e^{2\beta\mu - \beta U/4}, \tag{25}$$

for every site of the lattice. The energy per site is,

$$E = Z^{-1} \sum_{\alpha} \langle \alpha | \hat{\mathcal{H}} e^{-\beta \hat{\mathcal{H}}} | \alpha \rangle = \left(e^{-\beta U/4} + 2e^{\beta\mu + \beta U/4} + e^{2\beta\mu - \beta U/4} \right)^{-1}$$
$$\left(\frac{U}{4} e^{-\beta U/4} + 2(-\frac{U}{4} - \mu) e^{\beta\mu + \beta U/4} + (\frac{U}{4} - 2\mu) e^{2\beta\mu - \beta U/4} \right) \tag{26}$$

Meanwhile, the occupation is

$$\rho = \langle \hat{n} \rangle = Z^{-1} \sum_{\alpha} \langle \alpha | \quad \hat{n} e^{-\beta \hat{\mathcal{H}}} | \alpha \rangle = \left(e^{-\beta U/4} + 2e^{\beta\mu + \beta U/4} + e^{2\beta\mu - \beta U/4} \right)^{-1}$$
$$2 \left(e^{\beta\mu + \beta U/4} + e^{2\beta\mu - \beta U/4} \right) \tag{27}$$

A plot of the density ρ versus chemical potential μ, Fig. 6 (left), exhibits one of the most fundamental features of the Hubbard model, namely the "Mott insulating gap". As μ increases the density increases, but, at sufficiently low temperature, gets stuck at half-filling, $\rho = 1$, for a range $-U/2 < \mu < +U/2$. This jump in μ reflects the fact that once there is one electron on the site, the cost to add a second electron requires an additional energy cost U. It is important to emphasize that this is an entirely different type of gap than that which occurs in a band insulator when a band is completely filled with two electrons per state and there is a range of energy in which there are no states before the bottom of the next band begins. The Mott gap occurs for an odd number of electrons per site, a situation which band theory would insist on resulting in a metal.

In addition to the Mott insulating gap, one of the central features of the Hubbard model is the presence of magnetism. As noted earlier, the energy of the empty and doubly occupied states is $+U/4$, while that of the singly occupied states is $-U/4$. Thus the formation of '' 'local moments' (sites with non-zero spin) is energetically favored. The local moment $\langle \hat{m}^2 \rangle = \langle (\hat{n}_\uparrow - \hat{n}_\downarrow)^2 \rangle$ is a good measure of this tendency- it takes on the value 0 for empty and doubly occupied sites and is 1 for single occupation. Plots of $\langle \hat{m}^2 \rangle$ versus U at fixed temperature T and versus temperature T at fixed U are shown in 6 (center) and 6 (right) respectively. Large U and low T result in perfect moment formation $\langle \hat{m}^2 \rangle \to 1$. A nonzero hopping t introduces additional quantum fluctuations. For finite U, $\langle \hat{m}^2 \rangle$ will not go to 1 even at $T = 0$.

Moment formation, such as we are observing in the single site limit, is a pre-requisite for magnetism, but one also needs the magnetic moments on different sites to align (ferromagnetism) or antialign (anti-ferromagnetism) to speak of long range order. The physical picture for antiferromagnetism is that electrons on neighboring sites with spins which are antiparallel can hop onto

each other, resulting in a second order lowering of energy proportional to t^2/U. This hopping is forbidden for electrons of parallel spin. Hence antiferromagnetism is favored. Ferromagnetism can also occur in the Hubabrd model, but is much harder to achieve (in the single band case we are considering here). It is not too difficult to do a mean field calculation, and this will reveal magnetic behavior. However, we will not describe that in this chapter.

Instead, we will note that one can easily compute the Greens function in the $t = 0$ limit (and also, actually, in the $U = 0$ limit). Much of the initial progress in many-body physics rested upon diagrammatic perturbation theory, where the central quantity is the Greens function. Understanding that technology is a long slog, so it is pleasant to be able to do a simple calculation of this somewhat mysterious object. Consider

$$G_\uparrow(\tau) \equiv \langle\, \hat{c}_\uparrow(\tau)\hat{c}^\dagger_\uparrow(0)\,\rangle$$

in this single site limit. Only two of the states, those with the up spin occupied, contribute. For simplicity we will focus on the case $\mu = 0$. It is straightforward to show that,

$$G_\uparrow(\tau) = \frac{e^{+\beta U/4}e^{-\tau U/2} + e^{-\beta U/4}e^{\tau U/2}}{2\,e^{\beta U/4} + 2\,e^{-\beta U/4}}.$$

The Green's function is related to the spectral density $A(\omega)$ by the relation,

$$G(\tau) = \int_{-\infty}^{+\infty} A(\omega)\frac{e^{-\omega\tau}}{e^{-\beta\omega}+1}\,d\omega.$$

If you plug in

$$A(\omega) = \frac{1}{2}\,(\,\delta(\omega - \frac{U}{2}) + \delta(\omega + \frac{U}{2})\,)$$

and do the integral you get precisely the $G_\uparrow(\tau)$ we computed. The spectral function of the $t = 0$ Hubbard model consists of two delta function peaks separated by U. $A(\omega)$ is the many-body counterpart of the single particle density of states in the non-interacting limit. The separation of $A(\omega)$ by U is then akin to a band gap which would occur in $N(\omega)$, and is thus sensibly referred to as the Mott gap.

7 Particle-Hole Transformations

Our final topic focuses on the implications of certain canonical transformations on the low temperature properties of the Hubbard model and its generalizations. We will assume here a familiarity with the ground state phase diagram of the repulsive Hubbard model, especially that it exhibits long range AF order at half-filling with the long range spin ordering being degenerate along any of S_x, S_y or S_z directions (Heisenberg universality class).

Let us begin by considering a 'partial' particle-hole transformation (PHT),

$$\hat{c}_{\mathbf{j}\downarrow} \rightarrow (-1)^{\mathbf{j}} \hat{c}^{\dagger}_{\mathbf{j}\downarrow} \tag{28}$$

in which only the down spin operators are affected. In writing Eq. 28 we assume we are on a bipartite lattice (see Sec. 3.3) so that the symbol $(-1)^{\mathbf{j}}$ takes on the value $+1$ for $\mathbf{j} \in \mathcal{A}$ and -1 of $\mathbf{j} \in \mathcal{B}$. Under this transformation, the kinetic energy remains unchanged because, although it interchanges the order of the creation and destruction operators in the hopping, that reversal can be undone by invoking the anticommutation relations. The resulting minus sign is precisely canceled by the signs from the $(-1)^{\mathbf{j}}$ terms, as long as only near neighor hopping occurs (so that one site is in $\mathcal{A}$ and the other is in $\mathcal{B}$).

What does the PHT do to the potential energy? The down spin density $\hat{n}_{\mathbf{j}\downarrow} \leftrightarrow 1 - \hat{n}_{\mathbf{j}\downarrow}$ and, as a consequence the sign of U is reversed, mapping attraction to repulsion and vice-versa. Notice that writing the interaction in particle-hole symmetric form makes this observation especially easy to discern.

Finally, consider the chemical potential term. As noted immediately above, the down spin density (but not the up spin density) picks up a minus sign. The roles of charge and spin operators are interchanged $\hat{n}_{\mathbf{j}\uparrow} + \hat{n}_{\mathbf{j}\downarrow} \leftrightarrow \hat{n}_{\mathbf{j}\uparrow} - \hat{n}_{\mathbf{j}\downarrow}$. Thus the chemical potential term in $\hat{\mathcal{H}}$, $-\mu(\hat{n}_{\mathbf{j}\uparrow} + \hat{n}_{\mathbf{j}\downarrow})$ becomes $-\mu(\hat{n}_{\mathbf{j}\uparrow} - \hat{n}_{\mathbf{j}\downarrow})$ which is a Zeeman energy. Thus, $\mu \leftrightarrow B_z$ under this PHT.

To see how useful this mapping is, let's look at how physical observables are transformed. We note that because Eq. 28 applies only to the down spin operators, correlations of the Z component of spin map onto density correlations. On the other hand, the XY spin operators map onto s-wave pairing $\hat{c}^{\dagger}_{\mathbf{j}\uparrow}\hat{c}_{\mathbf{j}\downarrow} \leftrightarrow \hat{c}^{\dagger}_{\mathbf{j}\uparrow}\hat{c}^{\dagger}_{\mathbf{j}\downarrow}$.

With those mappings in place, the connections between the attractive and repulsive Hubbard models become clear. The fact that the square lattice repulsive Hubbard model has degenerate Z and XY antiferromagnetic spin order in its ground state at half-filling immediately implies the degeneracy of charge density wave and superconducting correlations in the attractive case. This is not at all an obvious thing if we just thought about the attractive model in isolation.

But there is even more to glean here: In a repulsive Hubbard model with antiferromagnetic order, a Zeeman field B_z causes AF Heisenberg spins to 'lie down' and order in the XY plane, perpendicular to the field. This is so because spins in the XY plane can tilt upwards into the Z direction and lower their energy linearly in the out of plane angle, whereas the disruption to the AF results in an energy cost which is quadratic in the angle. If the AF order were in the Z direction, tilting the spins would pick up only a quadratic field energy. The key obervation is then to note that when we do the PHT such a Zeeman term in the $+U$ model becomes a chemical potential in the $-U$ model. The doped attractive Hubbard model is thus seen to have a tendency for s-wave superconducting order. Indeed, because the field in the z direction reduces the universality class from Heisenberg to XY, the transition to s-wave SC order can occur at finite temperature.

This mapping and its consequences for *conventional* superconductivity have been known for nearly four decades. We will now show how an alternate canonical transformation lends similar insight into *exotic* superconductivity, something only realized recently [21].

To see this, let's consider a canonical transformation,

$$\hat{c}_{\mathbf{j}\downarrow} \to (-1)^{\mathbf{j}}\, \hat{c}_{\mathbf{j}\downarrow} \tag{29}$$

which is similar to that of Eq. 28 in having the staggered phase factor $(-1)^{\mathbf{j}}$, and acting only on the down spins, but lacks the transformation from particle to holes. Applying this to the attractive Hubbard model results in

$$\hat{\mathcal{H}}_{\sigma_z} = -t \sum_{\langle \mathbf{ij} \rangle} \sum_{\alpha\beta} \hat{c}^{\dagger}_{\mathbf{i}\alpha} \sigma_z^{\alpha\beta} \hat{c}_{\mathbf{j}\beta} - \mu \sum_{i,\alpha} \hat{n}_{\mathbf{i}\alpha} + U \sum_{\mathbf{i}} (\hat{n}_{\mathbf{i}\uparrow} - \frac{1}{2})(\hat{n}_{\mathbf{i}\downarrow} - \frac{1}{2}) \tag{30}$$

The Pauli matrix σ_z has spin indices α, β and result in hopping amplitudes for the spin-up and spin-down fermions differing in sign.

We can now infer the properties of this 'σ_z Hubbard model' from those of the attractive Hubbard model. While the CDW correlations map into themselves, the s-wave SC phase is altered. Specifically, the on-site pairing transforms as $\Delta_{\mathbf{j}} = c_{\mathbf{j}\downarrow} c_{\mathbf{j}\uparrow} \to \Delta_{\mathbf{j}} = (-1)^{\mathbf{j}} c_{\mathbf{j}\downarrow} c_{\mathbf{j}\uparrow}$. Therefore, the pairing remains on-site but with an alternating sign, indicating that the system displays s-wave pair density wave (PDW) superconductivity: The pairing function can be written as $\Delta^{\dagger} = \frac{1}{\sqrt{N}} \sum_j (-1)^{\mathbf{j}} c^{\dagger}_{\mathbf{j}\uparrow} c^{\dagger}_{\mathbf{j}\downarrow} = \frac{1}{\sqrt{N}} \sum_{\mathbf{k}} c^{\dagger}_{\mathbf{k}\uparrow} c^{\dagger}_{-\mathbf{k}+\mathbf{K}_0\downarrow}$ with $\mathbf{K}_0 = (\pm\pi, \pm\pi)$. Since we know the attractive Hubbard model has s-wave pairing, the σ_z Hubbard model must necessarily have a low temperature s-wave (singlet) PDW phase, in which an electron at momentum $\mathbf{k}$ pairs up with another at momentum $-\mathbf{k} + \mathbf{K}_0$, resulting in a Cooper pair carrying non-zero momentum.

An analogous mapping of the magnetism in the repulsive Hubbard model shows that the repulsive σ_z Hubbard model has a d-wave (triplet) PDW low temperature phase. These observations are quite remarkable. A PHT transformation, combined with the known phase diagram of the conventional Hubbard model, has revealed a microscopic model, the σ_z Hubbard model, which rigorously possesses pairing with non-zero momentum.

8 Concluding Remarks

The Hubbard model was developed to explain some most fundamental many-body phenomena in condensed matter physics- the mysterious Mott insulating behavior and magnetism in transition metal oxides. Several decades later, it emerged as one of the leading theories of d-wave superconductivity in the cuprates, and appears to hold insight into related stripe formation. After two further decades the Hubbard model re-invented itself yet again in AMO community. One might think such a powerful theory would also be inaccessible. We hope these notes have proven that is not the case. We also hope that they suggest the Hubbard model is not yet finished having something to say about new condensed matter problems- including non-Hermitian physics, quantum state transfer, and pair density wave phases.

References

[1] Patrik Fazekas: *Lecture Notes on Electron Correlation and Magnetism* (World Scientific, Singapore, 1999)

[2] T. Esslinger, Annual Review of Condensed Matter Physics 1, 129 (2010).

[3] L. Tarruell and L. Sanchez-Palencia, Comptes Rendus Physique 19, 365 (2018).

[4] J. Zaanen and O. Gunnarsson, Physical Review B 40, 7391, (1989).

[5] J.P.F. LeBlanc *etal*, Physical Review X 5, 041041 (2015).

[6] S.R. White and D.J. Scalapino, Physical Review Letters 91, 136403, (2003).

[7] K. ChŃg, J. Carrasquilla, R.G. Melko, and E. Khatami, Physical Review X 7, 031038, (2017).

[8] D.P. Arovas, E. Berg, S.A. Kivelson, and S. Raghu, Annual Review of Condensed Matter Physics 13, 239 (2022).

[9] E. Abrahams, P.W. Anderson, D.C. Licciardello, and T.V. Ramakrishnan, Physical Review Letters 42, 673 (1979).

[10] F. Evers and A.D. Mirlin, Reviews of Modren Physics 80, 1355 (2008).

[11] Reviews of Modern Physics 3, 251 (2001).

[12] A.A. Maradudin, P. Mazur, E.W. Montroll, and G.H. Weiss, Reviews of Modern Physics 30, 175, (1958).

[13] J. Feinberg and A. Zee, Nuclear Physics B504, 579 (1997).

[14] C.M. Bender, Reports on Progress in Physics 70, 947 (2007).

[15] Y. Ashida, Z. Gong, and M. Ueda, Advances in Physics 69, 249 (2020).

[16] Indeed, by making the identifical of the number of sites N to $2j+1$ and the site index n to $m+j+1$ it is simple to show $n = 1, 2, \cdots N$ and $\sqrt{j(j+1) - m(m+1)} = \sqrt{n(N-n)}$.

[17] M. Christandl, N. Datta, A. Ekert, and A.J. Landahl, Physical Review Letters 92, 187902 (2004).

[18] A. Kay, International Journal of Quantum Information 08, 641 (2010).

[19] X. Li, Y. Ma, J. Han, T. Chen, Y. Xu, W. Cai, H. Wang, Y.P. Song, Z-Y.. Xue, Z-q. Yin, and L. Sun, Physical Review Applied 10, 054009 (2018).

[20] L. Xiang *etal*, Nature Communications 15, 4918 (2024).

[21] A demonstration of exotic η-pairing from such canonical transformations also has a long history. See C.N. Yang, Physical Review Letters 63, 2144 (1989). However the remarks which follow are first described in X. Zhu, J. Sun, S-S. Gong, W. Huang, S. Feng, R.T. Scalettar, and H. Guo, arXiv:2404.11043.